THE JOURNAL OF PHYSICAL CHEMISTRY B

Article

pubs.acs.org/JPCB

Aggregate Transitions in Mixtures of Anionic Sulfonate Gemini Surfactant with Cationic Ammonium Single-Chain Surfactant

Maozhang Tian,[†] Linyi Zhu,[†] Defeng Yu,[†] Yingxiong Wang,[†] Shufeng Sun,[‡] and Yilin Wang*[,†]

[†]Key Laboratory of Colloid and Interface Science, Beijing National Laboratory for Molecular Sciences (BNLMS), Institute of Chemistry, Chinese Academy of Sciences, Beijing 100190, China

[‡]Center for Biological Electron Microscopy, Institute of Biophysics, Chinese Academy of Sciences, Beijing 100101, China

ABSTRACT: Aggregation behaviors in mixtures of an anionic gemini surfactant 1,3-bis(*N*-dodecyl-*N*-propanesulfonate sodium)−propane ($C_{12}C_3C_{12}(SO_3)_2$) and a cationic single-chain surfactant cetyltrimethylammonium bromide (CTAB) have been investigated in aqueous solutions at pH 9.5 by turbidity, rheology, isothermal titration microcalorimetry (ITC), cryogenic transmission electron microscopy, and dynamic light scattering. Reversible aggregate transitions from spherical micelles to wormlike micelles, vesicles, and back to wormlike micelles and spherical micelles are successfully realized through fine regulation over the mixing ratio of surfactants, i.e., the anionic/cationic charge ratio. The five aggregate regions display distinguished phase boundaries so that the aggregate regions can be well controlled. From thermodynamic aspect, the ITC curves clearly reflect all the aggregate transitions and the related interaction mechanism. The self-assembling ability of the $C_{12}C_3C_{12}(SO_3)_2$/CTAB mixtures are significantly improved compared with both individual surfactants. Micelle growth from spherical to long wormlike micelles takes place at a relative low total concentration, i.e., 2.0 mM. The wormlike micelle solution at 10 mM or higher shows high viscosity and shear thinning property. Moreover, the $C_{12}C_3C_{12}(SO_3)_2$/CTAB mixtures do not precipitate even at 1:1 charge ratio and relative high concentration. It suggests that applying gemini surfactant should be an effective approach to improve the solubility of anionic/cationic surfactant mixtures and in turn may promote applications of the surfactant mixtures.

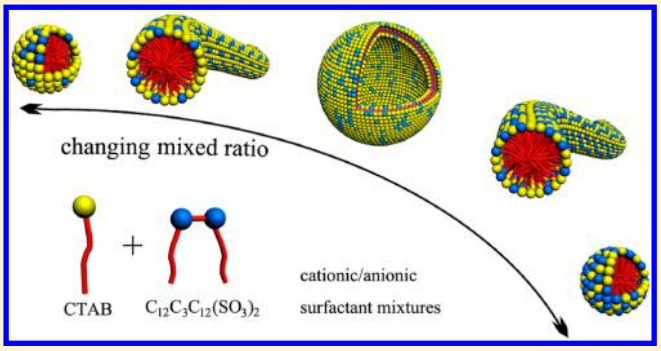

INTRODUCTION

Surfactants in solutions can self-assemble into well-organized structures in the nanometer or micrometer scale, such as micelles, vesicles, and lamellar phase. These self-assemblies display different influences on the rheology of solutions.[1−14] Normally spherical micelles and vesicles cannot obviously improve the rheological property of solutions, while wormlike micelles can entangle into a transient network showing viscoelastic behaviors analogous to polymer solutions above a threshold concentration.[4] However, different from polymers which are conjunct by covalent bonds, wormlike micelles of surfactants induced by intermolecular interactions can reversibly break and re-form under prevailing physicochemical conditions and therefore exist in a dynamic equilibrium.[5−7] So they are called "living" polymers. In addition, with good detergency and easily tunable microstructures, wormlike micelles of surfactants have become ubiquitous to industrial processes and emerging technologies.[1−3] All these have excited great interest of researchers to endeavor to build viscoelastic wormlike micelles in surfactant systems.[8−15]

Formation of wormlike micelles is strongly dependent on surfactant molecule geometry. Wormlike micelles can be formed by individual surfactants with packing parameter varying from 1/3 to 1/2.[1,2,16] Accordingly, many surfactants forming wormlike micelles were synthesized and studied. For instance, a series of surfactants with long hydrophobic chain and zwitterionic headgroup with amino bonds have been shown to form wormlike micelles with good viscoelastic properties.[17,18] Introducing various salts into long-tail ionic surfactants[9,19−24] and mixing cationic and anionic surfactants[25−27] are another two facile approaches to construct wormlike micelles.

Benefiting from "synergism", cationic/anionic surfactant mixtures normally present significantly enhanced self-assembly properties and thereby attract more attention.[5,28−33] For decades, systematic investigations on cationic/anionic surfactant mixtures have been implemented to construct aggregates with desired properties.[34−38] It is well-known that mixing cationic/anionic surfactants can weaken electrostatic interaction among charged headgroups and in turn the weakened electrostatic interaction can promote micelle growth and finally form wormlike micelles.[5,25−27] An intriguing feature of such wormlike micellar systems is the nonmonotonic changing trend in rheological property at high surfactant concentration.[5,25,26]

Received: October 11, 2012
Revised: November 29, 2012
Published: December 3, 2012

Kaler's group[25] succeeded in constructing wormlike micelles in the mixtures of sodium oleate (NaOA) and octyltrimethylammonium bromide (OTAB). The mixed solutions are viscous at the OTAB weight fraction ranging from 0.2 to 0.8. Meanwhile, there is a remarkably high viscosity peak at a weight ratio of 70/30 NaOA/OTAB, while the viscosity is considerably low as either surfactant is in great excess. Koehler et al.[5] investigated the formation of wormlike micelles in the mixtures of a cationic surfactant cetyltrimethylammonium tosylate (CTAT) and an anionic surfactant sodium dodecyl benzenesulfonate (SDBS). It was also found that there is a maximum value at the CTAT molar fraction of 0.3 in the plot of zero shear rate viscosity (η^0) against total surfactant concentration, just like in most of the mixtures of salts and surfactants.[19] This work also revealed that viscosity decreasing after the maximum is caused by the aggregate transition from long cylinder micelles to branched wormlike micelles.

Even if wormlike micelles of mixed surfactants have been widely studied, how to conveniently and efficiently construct wormlike micelles is still a challenging target pursued in the surfactant field. Gemini surfactants,[39,40] constructed by two hydrophobic chains and two head groups covalently connected by a spacer group, have been proved to be superior to corresponding single-chain surfactants due to their strong self-assembly ability and enriched self-assembling structures. Moreover, Zana et al.[41] have proved that cationic gemini surfactants alkanediyl-α,ω-bis(dodecyldimethylammonium bromide) ($C_{12}C_mC_{12}Br_2$) with short spacer group can self-assemble into wormlike micelles. In our previous work,[42] an anionic gemini surfactant 1,3-bis(*N*-dodecyl-*N*-propanesulfonate sodium)-propane ($C_{12}C_3C_{12}(SO_3)_2$) with a 3-carbon length spacer was synthesized and studied. This surfactant has a remarkably low critical micellar concentration (cmc) and can self-assemble into wormlike micelles with addition of divalent metal ion (Ca^{2+}).[43] Therefore, $C_{12}C_3C_{12}(SO_3)_2$ should be an excellent candidate to construct wormlike micelles with cationic surfactants. Cetyltrimethylammonium bromide (CTAB) is a cationic quaternary ammonium surfactant with a long hydrocarbon chain and it self-assembles into spherical micelles at very low concentration.[44] The $C_{12}C_3C_{12}(SO_3)_2$/CTAB mixture is thus expected to be a very efficient self-assembling system.

In this work, the mixtures $C_{12}C_3C_{12}(SO_3)_2$ with CTAB have been studied at pH 9.5 in aqueous solution and fine adjusting of the structures of the mixed aggregates was realized through varying the mixed ratio. At the pH 9.5 used, the sulfonate groups of $C_{12}C_3C_{12}(SO_3)_2$ are completely deprotonated and each molecule carries two negative charges as a gemini surfactant. Turbidity, rheology, dynamic light scattering (DLS), and cryogenic transmission electron microscopy (Cryo-TEM) have been employed to characterize the aggregate transitions and viscosity properties in the mixed $C_{12}C_3C_{12}(SO_3)_2$/CTAB aqueous solution. The transitions were observed from spherical micelles to wormlike micelles, then to vesicles, and finally back to wormlike micelles and spherical micelles. Isothermal titration microcalorimetry (ITC) was employed as an attempt for following the enthalpy change in the aggregate transitions. Microcalorimetry is a powerful tool for investigating the intermolecular interactions in physical and chemical processes from the thermodynamic aspect.[45−54] It has been employed to study the transition between vesicles and micelles in cationic/anionic surfactants mixtures.[45,50,51] But applying it for characterizing the transition from spherical micelles to wormlike micelles has never been reported. Herein, ITC measurement was successfully managed to characterize the enthalpy change during the transitions from spherical micelles to wormlike micelles and vesicles in the cationic/anionic surfactants mixtures. The results help to further understand the intermolecular interactions in the transitions and provide a guidance to elaborately adjust the aggregate structures in mixtures of cationic/anionic surfactants.

EXPERIMENTAL SECTION

Materials. Anionic gemini surfactant 1,3-bis(*N*-dodecyl-*N*-propanesulfonate sodium)-propane ($C_{12}C_3C_{12}(SO_3)_2$) was synthesized and purified according to previous literature.[42] The cationic surfactant CTAB was purchased from TCI Co. with purity higher than 99% and was recrystallized before use. Water used for preparing the mixture solution in all experiments was from Milli-Q equipment. The resistivity of the Milli-Q water was 18.2 MΩ cm. All experiments were carried out at pH 9.5.

Turbidity Measurements. Turbidity measurements were used to study the tendency of the size variation of aggregates in solutions and were carried out with a Shimadau 1601 PC UV/vis spectrometer. The turbidity of the $C_{12}C_3C_{12}(SO_3)_2$/CTAB mixtures was determined by UV absorbance at 450 nm at 25.0 ± 0.1 °C. A cuvette with 1 cm pathway was used.

Isothermal Titration Microcalorimetry (ITC). A TAM 2277-201 isothermal titration microcalorimeter (Thermometric AB, Jarfalla, Sweden) was used to measure the enthalpy change of the aggregate transitions occurred in the mixed solution. The sample cell and the reference cell of the microcalorimeter were initially loaded with water or surfactant solution. During the whole titration process, another surfactant solution was injected consecutively into the stirred sample cell using a 500 μL Hamilton syringe controlled by a Thermometric 612 Lund pump until the desired concentration range had been covered. The system was stirred at 60 rpm with a gold propeller, and the interval between two injections was long enough for the signal to return to the baseline. The observed enthalpy (ΔH_{obs}) was obtained by integrating the areas of the peaks in the plot of thermal power against time. The reproducibility of experiments was within ±4%. All the measurements were performed at 25.00 ± 0.01 °C.

Dynamic Light Scattering (DLS). DLS was used to determine the size of aggregates and were carried out with an LLS spectrometer (ALV/SP-125) with a multi-τ digital time correlator (ALV-5000). A solid-state He−Ne laser (output power of 22 mW at λ = 632.8 nm) was used as a light source, and the measurements were conducted at a scattering angle of 90°. The freshly prepared samples were injected into a 7 mL glass bottle through a 0.45 μm filter prior to measurements. The correlation function of scattering data was analyzed via the CONTIN method to obtain the distribution of diffusion coefficients (D) of the solutes, and then, the apparent equivalent hydrodynamic radius (R_h) was determined using the Stokes−Einstein equation $R_h = kT/6\pi\eta D$, where k is the Boltzmann constant, T is the absolute temperature, and η is the solvent viscosity. All the measurements were performed at 25.00 ± 0.05 °C.

Rheology Measurement. The rheological properties of the mixed solutions were investigated at 25.00 ± 0.05 °C with a ThermoHaake RS300 rheometer (cone and plate geometry of 35 mm in diameter with the cone gap equal to 0.105 mm). A solvent trap was used to avoid water evaporation. Frequency

dx.doi.org/10.1021/jp310065y | J. Phys. Chem. B 2013, 117, 433−440

spectra were conducted in the linear viscoelastic regime of the samples determined from dynamic strain sweep measurements. For the solutions with low viscosity, a double-gap cylindrical sensor system with an outside gap of 0.30 mm and an inside gap of 0.25 mm was employed.

Cryogenic Transmission Electron Microscopy (Cryo-TEM). The samples were embedded in a thin layer of vitreous ice on freshly carbon-coated holey TEM grids by blotting the grids with filter paper and then plunging them into liquid ethane cooled by liquid nitrogen. Frozen hydrated specimens were imaged by using an FEI Tecnai 20 electron microscope (LaB6) operated at 200 kV in the low dose mode (about 2000 e/nm^2) and the nominal magnification of 50 000. For each specimen area, the defocus was set to 1−2 μm. Images were recorded on Kodak SO 163 films and then digitized by Nikon 9000 with a scanning step 2000 dpi corresponding to 2.54 Å/pixel.

RESULTS AND DISCUSSION

Turbidity and Rheological Properties. Figure 1a shows the turbidity of $C_{12}C_3C_{12}(SO_3)_2$/CTAB solutions plotted against the molar fraction of $C_{12}C_3C_{12}(SO_3)_2$ (X_g) at total surfactant concentration C_T of 2.0 mM and 10.0 mM. The turbidity curves show similar variation tendency for C_T = 2.0 and 10.0 mM, and strongly depend on X_g. When either $C_{12}C_3C_{12}(SO_3)_2$ or CTAB is in great excess (X_g < 0.22 and X_g > 0.43), the solutions are transparent with a turbidity very close to zero. Because the surfactant concentrations are above the cmc of $C_{12}C_3C_{12}(SO_3)_2$ and CTAB, the $C_{12}C_3C_{12}(SO_3)_2$/CTAB mixtures should have self-assembled into small aggregates, but the size is not large enough to affect the solution turbidity. When X_g is in region 0.22−0.43, the turbidity increases remarkably and reach a maximum, where the solution is bluish, indicating the formation of large aggregates. For C_T = 2.0 mM, the $C_{12}C_3C_{12}(SO_3)_2$/CTAB solutions are homogeneous and no precipitation takes place even at the charge ratio very close to 1:1 (i.e., X_g = 0.33). For C_T = 10.0 mM, the mixed solution only precipitates at a very narrow region around 1:1 charge ratio.

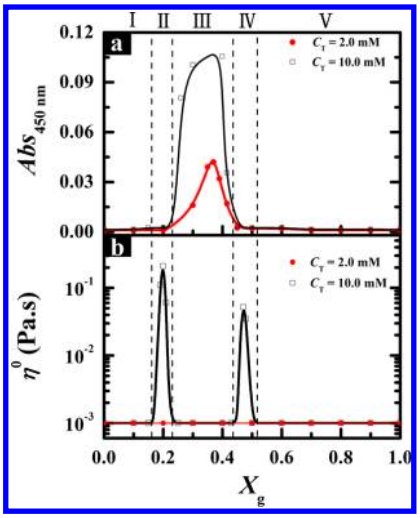

Figure 1. (a) Turbidity and (b) zero-shear viscosity η^0 of $C_{12}C_3C_{12}(SO_3)_2$/CTAB solutions plotted against the molar fraction of $C_{12}C_3C_{12}(SO_3)_2$ (X_g) at C_T = 2.0 and 10.0 mM.

The variation of zero-shear viscosity η^0 for the corresponding solutions above is shown in Figure 1b. The η^0 values are derived from the curves of the steady viscosity versus shear rate. At C_T = 2.0 mM, the viscosity of the mixed solutions is very low and close to that of water (∼1.0 mPa·s). So the mixed solutions behave as Newtonian fluid over the whole X_g. At C_T = 10.0 mM, the steady shear viscosity plots at different X_g are shown in Figure 2. Clearly, the mixed solution is viscous in two regions;

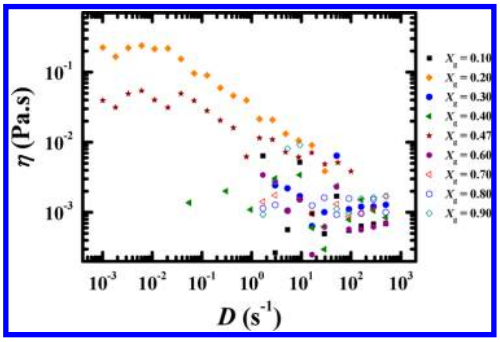

Figure 2. Steady shear viscosity plots for $C_{12}C_3C_{12}(SO_3)_2$/CTAB mixtures at different X_g (C_T = 10.0 mM).

i.e., X_g is located in 0.18−0.22 and 0.43−0.50, while the η^0 in other regions is close to the viscosity of water. The η^0 value reaches two maxima at X_g = 0.20 and 0.47, respectively. Interestingly, the two high-viscosity regions are just located in the transitional regions from low turbidity to high turbidity or from high turbidity to low turbidity. The mixed solutions with high viscosity display an ability to trap bubbles, suggesting that wormlike micelles may form in these two regions. To confirm the formation of wormlike micelles in these two regions, the solutions at X_g = 0.20 and 0.47 were chosen as representatives and their steady shear viscosities at different C_T were measured. The shear thinning properties of the mixed solutions at X_g = 0.20 and 0.47 cannot be clearly measured at low concentrations due to the sensitivity of the rheological equipment, but the results shown in Figure 3 indicate that the surfactant solutions with the total concentration beyond 10.0 mM show shear thinning properties, which is the typical characteristic of non-Newtonian fluids. The deviation from Newtonian behavior becomes pronounced and the zero-shear viscosity is greatly increased when the total concentration increases. When C_T reaches 80 mM, the low shear viscosity of the surfactant solution is as high as 15 and 2 Pa·s at X_g = 0.20 and 0.47, respectively. These viscosity properties further signify the formation of wormlike micelles in the regions.

In brief, on the basis of the turbidity and the viscosity curves, the $C_{12}C_3C_{12}(SO_3)_2$/CTAB mixtures can be divided into five regions according to X_g, which are 0−0.16 (I), 0.16−0.22 (II), 0.22−0.43 (III), 0.43−0.51 (IV), and 0.51−1.00 (V), as noted by the dashed lines in Figure 1. In another words, a series of the aggregate transitions can be induced through changing the X_g.

Size and Morphology of Aggregates. To have a deep insight into the aggregation behaviors in the five regions determined above, DLS and Cryo-TEM were employed to characterize the size and morphology of the aggregates. Because the aggregate transitions are the same at C_T = 2.0 and 10.0 mM, the situations at C_T = 2.0 mM are shown as representatives. The size distributions of the representative samples in the five regions are shown in Figure 4, and the corresponding Cryo-TEM micrographs are presented in Figure 5.

dx.doi.org/10.1021/jp310065y | J. Phys. Chem. B 2013, 117, 433−440

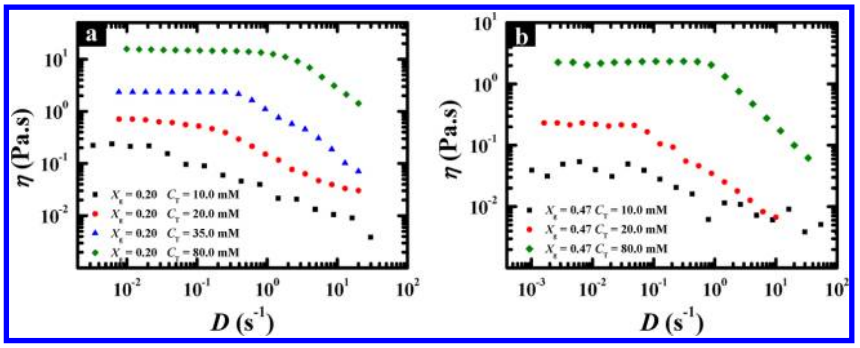

Figure 3. Steady shear viscosity plots for $C_{12}C_3C_{12}(SO_3)_2$/CTAB solutions at X_g = 0.20 and 0.47.

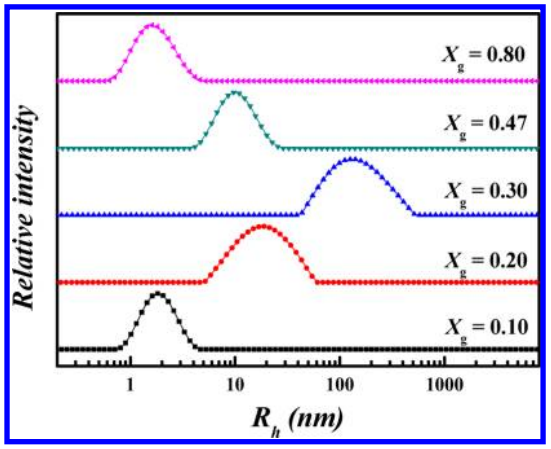

Figure 4. Size distributions of $C_{12}C_3C_{12}(SO_3)_2$/CTAB aggregates from DLS at C_T = 2.0 mM, and X_g = 0.10, 0.20, 0.30, 0.47, and 0.80.

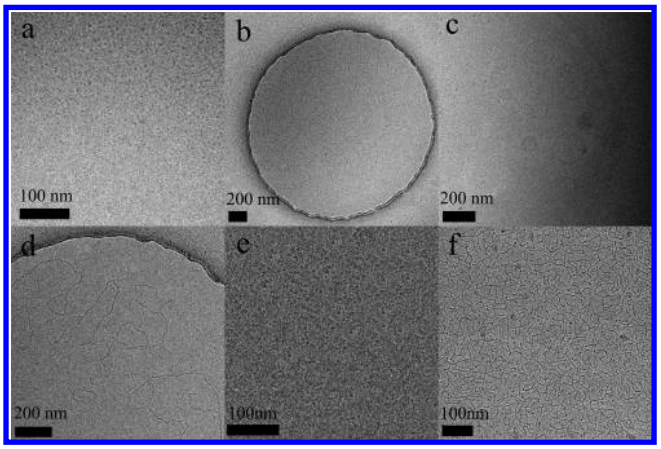

Figure 5. Cryo-TEM micrographs of the $C_{12}C_3C_{12}(SO_3)_2$/CTAB aggregates: for C_T = 2.0 mM, at X_g = 0.10 (a), 0.20 (b), 0.30 (c), 0.47 (d), and 0.80 (e); for C_T = 10.0 mM, X_g = 0.20 (f).

At X_g = 0.10 and C_T = 2.0 mM (in region I), a small size distribution of aggregates with R_h of ~2 nm exists in the DLS result and the Cryo-TEM image (Figure 5a) illustrate that the aggregates are small spherical micelles. This is in accordance with the transparent solution with low viscosity observed above.

At X_g = 0.20 and C_T = 2.0 mM (in region II), the DLS result shows that the R_h of the aggregates is ~20 nm, obviously larger than that of the spherical micelles. The Cryo-TEM images (Figure 5b) show that the aggregates are long wormlike micelles with a diameter about ~5 nm. Because the data were treated as spherical aggregates in the DLS measurements, the size from DLS cannot reflect the real situation of wormlike micelles. At this concentration, the wormlike micelles are rarely entangled with each other due to the low total concentration. So wormlike micelles can be observed but the viscosity is almost as that of water. However, in the same region, if C_T increases to 10.0 mM, the Cryo-TEM image (Figure 5f) indicates that the long wormlike micelles entangle into networks at this concentration, which results in the high viscosity.

At X_g = 0.30 and C_T = 2.0 mM (in region III), the DLS result indicates that the R_h of the aggregates is ~158 nm. The Cryo-TEM image (Figure 5c) shows that the aggregates are spherical vesicles and multilamillar vesicles. The formation of the large vesicles explains the sharp increase of the turbidity in Figure 1a.

At X_g = 0.47 and C_T = 2.0 mM (in region IV), the aggregates are almost the same as those in region II. The R_h of the aggregates from DLS is ~18 nm while the Cryo-TEM image (Figure 5d) shows that the aggregates are long wormlike micelles, which brings about the high viscosity to the solution. The situation of this region is very close to that in region II.

At X_g = 0.80 and C_T = 2.0 mM (in region V), the R_h value of aggregates from DLS is ~2 nm and the Cryo-TEM image (Figure 5e) illustrates that the aggregates are small spherical micelles. This means that the $C_{12}C_3C_{12}(SO_3)_2$/CTAB mixture returns to the aggregate structure and solution property in region I.

Combining the aforementioned results, the influence of X_g on the self-assembly behavior of the $C_{12}C_3C_{12}(SO_3)_2$/CTAB mixtures can be summarized as follows. When either $C_{12}C_3C_{12}(SO_3)_2$ or CTAB is in great excess, the mixtures self-assemble into spherical micelles. Adding more oppositely charged surfactant into the mixed solutions leads to the growth of the micelles and generates wormlike micelles in the system. While the mixing ratio gets close to 1:1 charge ratio, the wormlike micelles transfer into spherical vesicles. In the following text, we will study the intermolecular interaction driving these aggregate transitions from thermodynamic aspect.

Interactions in Aggregate Transitions Studied by ITC.

ITC measurements were employed to characterize the enthalpy changes during the aggregate transitions in the $C_{12}C_3C_{12}(SO_3)_2$/CTAB solutions. Figure 6 presents the observed enthalpy ΔH_{obs} against X_g at C_T = 2.0 and 10.0 mM. The measurements were carried out by titrating 2.0 or 10.0 mM $C_{12}C_3C_{12}(SO_3)_2$ solution into CTAB solution or $C_{12}C_3C_{12}(SO_3)_2$/CTAB solution at the same total concentration. During the titrations, the total surfactant concentration of the final solution in the sample cell did not change; i.e., the total concentration was 2.0 or 10.0 mM; however, the $C_{12}C_3C_{12}(SO_3)_2$ molar fraction X_g gradually changed with the titrations. Because the surfactant concentrations are above the

dx.doi.org/10.1021/jp310065y | J. Phys. Chem. B 2013, 117, 433−440

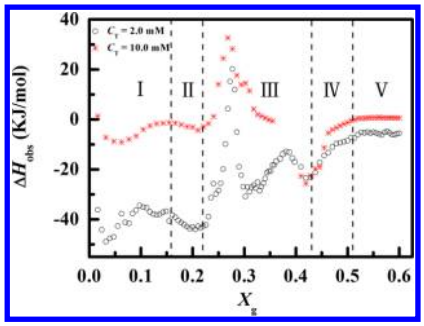

Figure 6. Observed enthalpy changes ΔH_{obs} by titrating 2.0 mM $C_{12}C_3C_{12}(SO_3)_2$ into 2.0 mM CTAB solutions (black circles) (a), and by titrating 10.0 mM $C_{12}C_3C_{12}(SO_3)_2$ into 10.0 mM CTAB solutions (red stars) (b).

cmc of $C_{12}C_3C_{12}(SO_3)_2$ and CTAB, respectively, the surfactants self-assembled into micelles in the initial solutions. As shown in Figure 6, both the ITC curves have very similar variation patterns. The differences mainly exist in the ΔH_{obs} values. Obviously, the ΔH_{obs} values strongly depend on X_g. In order to understand the interaction of $C_{12}C_3C_{12}(SO_3)_2$ with CTAB, the ΔH_{obs} of titrating 2.0 and 10.0 mM $C_{12}C_3C_{12}(SO_3)_2$ into water were also studied for comparison, shown in Figure 7.

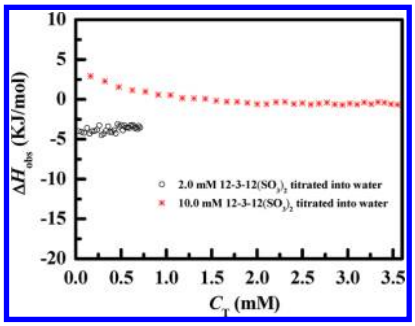

Figure 7. Observed enthalpy changes ΔH_{obs} by titrating 2.0 mM $C_{12}C_3C_{12}(SO_3)_2$ (black circles) (a) and 10.0 mM $C_{12}C_3C_{12}(SO_3)_2$ (red stars) solution into water (b).

Because both the ITC curves at C_T = 2.0 and 10.0 mM have very similar variation patterns, the following discussion about the ITC curves will take the case at C_T = 2.0 mM as an example.

When X_g falls in the region 0−0.16 (I), the observed enthalpy ΔH_{obs} is exothermic, and with the increase of X_g from 0 to 0.16, the exothermic ΔH_{obs} value increases with initial addition of $C_{12}C_3C_{12}(SO_3)_2$ and starts to decrease thereafter. In this region, CTAB are rich in the mixed micelles and the mixed micelles are small spherical micelles as revealed above. The interaction processes are mainly included: the dissociation of the $C_{12}C_3C_{12}(SO_3)_2$ micelles into monomers and the further dilution, the binding of the $C_{12}C_3C_{12}(SO_3)_2$ monomers with the CTAB micelles, and the formation of the $C_{12}C_3C_{12}(SO_3)_2$/CTAB mixed micelles. Because the dissociation of the $C_{12}C_3C_{12}(SO_3)_2$ micelles into monomers and the further dilution is reflected in the ITC curve of titrating 2.0 mM $C_{12}C_3C_{12}(SO_3)_2$ into water (Figure 7a), which is only slightly exothermic, the large exothermic ΔH_{obs} values in Figure 6a are mainly attributed to the latter two kinds of interactions, i.e., the binding of $C_{12}C_3C_{12}(SO_3)_2$ with CTAB by electrostatic interaction between oppositely charged headgroups, and the formation of the $C_{12}C_3C_{12}(SO_3)_2$/CTAB mixed micelles driven by hydrophobic interactions among the hydrocarbon chains. When initially adding $C_{12}C_3C_{12}(SO_3)_2$ into CTAB, these two interactions should show strong tendency, so the resultant exothermic ΔH_{obs} values increase. With the increase of X_g, the net charges of the mixed $C_{12}C_3C_{12}(SO_3)_2$/CTAB micelles gradually decrease, which gradually weakens the electrostatic interaction of added $C_{12}C_3C_{12}(SO_3)_2$ with the mixed micelles, and thus the further addition of $C_{12}C_3C_{12}(SO_3)_2$ leads to a declining tendency of the exothermic ΔH_{obs} values thereafter.

When X_g is located in the region 0.16−0.22 (II), the exothermic ΔH_{obs} value increases progressively. In this region, the spherical micelles grow into long wormlike micelles. Because more and more $C_{12}C_3C_{12}(SO_3)_2$ molecules are involved in the mixed $C_{12}C_3C_{12}(SO_3)_2$/CTAB micelles, the mixed micelles have lower charge density and the headgroups get closer to each other, which drives the hydrocarbon chains to pack more tightly and results in the growth of the micelles and the formation of long wormlike micelles. Although the decreasing net charges of the mixed $C_{12}C_3C_{12}(SO_3)_2$/CTAB micelles will result in a declining exothermic ΔH_{obs} value, the transitions of spherical micelles to wormlike micelles obviously make ΔH_{obs} to be more exothermic.

When X_g is in region 0.22−0.43 (III), the ITC curve displays a complicated pattern. At the beginning, the ΔH_{obs} value sharply changes from significant exothermic to endothermic. After a maximum, the endothermic ΔH_{obs} value abruptly changes to exothermic. Thereafter, the exothermic ΔH_{obs} value experiences a decrease and then a decrease process. Although the ITC curve varies in such a complicated way, only large spherical vesicles exist in the Cryo-TEM image of this region. Combining the results from turbidity, viscosity, DLS, and Cryo-TEM, the region should correspond to the transition from wormlike micelles to vesicles, and the ITC curves can be explained as below. With the increase of X_g beyond 0.22, the net charges of the mixed $C_{12}C_3C_{12}(SO_3)_2$/CTAB micelles continue to decrease and the net charges become low enough to make the surfactant headgroups get very close with each others. Correspondingly, the hydrophobic interaction of the surfactant molecules is greatly strengthened. These interactions lead to the transition from wormlike micelles to vesicles and normally result in an increase in the exothermic ΔH_{obs} value. However, the experimental results indicate that the ΔH_{obs} changes to endothermic. This phenomenon suggests that the transition from wormlike micelle to vesicles may be accompanied with strong dehydration or deionization of the surfactants. The maximum of the endothermic ΔH_{obs} value implies that the transition from wormlike micelles to vesicles may come to an end at the point. So afterward the dehydration and deionization may be greatly weakened, and the added anionic $C_{12}C_3C_{12}(SO_3)_2$ molecules only bind with the cationic CTAB in the vesicles but do not change the structure of aggregates. These factors change the endothermic ΔH_{obs} value to be an increasing exothermic ΔH_{obs} value. At X_g = 0.33, the charge ratio of $C_{12}C_3C_{12}(SO_3)_2$/CTAB is very nearly 1:1. Beyond this point, the added $C_{12}C_3C_{12}(SO_3)_2$ causes the vesicles to start carrying on negative charges. The titrated anionic surfactant $C_{12}C_3C_{12}(SO_3)_2$ binds with the vesicles and joins the vesicles. This process is exothermic as revealed by the ITC curves. However, with the increase of the negative charges on vesicles, electrostatic repulsion between the newly added $C_{12}C_3C_{12}(SO_3)_2$ and the $C_{12}C_3C_{12}(SO_3)_2$ already in vesicles reduces the exothermic ΔH_{obs} value. From X_g = 0.38, there is an exothermic increasing step. This point just corresponds to

dx.doi.org/10.1021/jp310065y | J. Phys. Chem. B 2013, 117, 433−440

the maxima of the turbidity curves, i.e., afterward the size of aggregates in the system begins to decrease. Because at this stage the viscosity does not vary, which indicates the wormlike micelles have not yet formed, the decrease of the aggregate size may come from the dissociation of the large vesicles into small ones driven by the electrostatic repulsion of the headgroups. This process may be the reason of the increase of the exothermic ΔH_{obs} value.

When X_g is located in region 0.43−0.51 (IV), the exothermic ΔH_{obs} value experiences a decreasing process and becomes close to zero at the end of this region. The Cryo-TEM, DLS, and viscosity results indicate that the vesicles transfer into wormlike micelles in this region. Because in this region the viscosity presents an increase and then a decrease process, the amount of the wormlike micelles must undergo the same process. The process originates from the enhancement of electrostatic repulsion between the surfactant headgroups. When more and more $C_{12}C_3C_{12}(SO_3)_2$ are added into the $C_{12}C_3C_{12}(SO_3)_2$/CTAB vesicles, the vesicles carry too many negative charges and the strong electrostatic repulsion between these charges drives the vesicles to transfer into wormlike micelles, and finally into small spherical micelles. During these transitions, hydrophobic interaction is weakened and the vesicle dissociation may be accompanied with strong hydration and ionization of the aggregates. The conjoint actions of all these factors lead to the declination of the exothermic ΔH_{obs} value.

Finally, when X_g is in region 0.51−1.00 (V), the ΔH_{obs} value is close to zero and almost does not change anymore. As presented above, the mixed $C_{12}C_3C_{12}(SO_3)_2$/CTAB system already completely transfers into small spherical micelles in this region. The spherical micelles become rich in $C_{12}C_3C_{12}(SO_3)_2$, and the addition of $C_{12}C_3C_{12}(SO_3)_2$ only changes the composition of the spherical micelles. So the curves coincide with the curves of titrating $C_{12}C_3C_{12}(SO_3)_2$ into water.

In summary, the variations in the ITC curves agree well with the variations obtained by turbidity, rheology DLS, and Cryo-TEM experiments. The emergence of manifold energy alterations reveals the variation of the molecular interaction in the aggregate transitions.

Proposed Models of Aggregate Transitions. Combining all the results and discussion above, the aggregate transitions in the $C_{12}C_3C_{12}(SO_3)_2$/CTAB mixture induced by varying mixing ratio can be summarized with the simplified models shown in Figure 8. The mixing ratio determines the charge ratio. That is to say, controlled aggregate transitions in the $C_{12}C_3C_{12}(SO_3)_2$/CTAB mixtures are realized through adjusting electrostatic interaction between oppositely charged surfactants. On either increasing the ratio of $C_{12}C_3C_{12}(SO_3)_2$ or CTAB in the mixtures, the mixtures undergo the same process of aggregate transitions, i.e., spherical micelles, wormlike micelles, vesicles, and then wormlike micelles and spherical micelles again. These five phase regions have clearly distinguished boundaries.

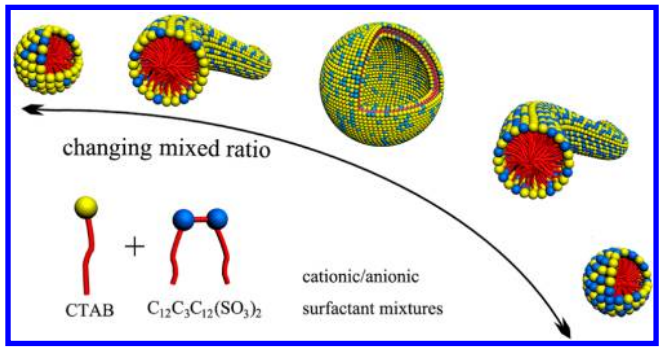

Figure 8. Simplified models of the aggregate transitions in the $C_{12}C_3C_{12}(SO_3)_2$/CTAB mixtures.

In general, aggregate transitions depend on the variation of surfactant packing parameter. Before mixing, $C_{12}C_3C_{12}(SO_3)_2$ and CTAB form micelles at the concentration used here. Varying the mixing ratio of $C_{12}C_3C_{12}(SO_3)_2$/CTAB will alter the average packing parameter of the mixed surfactants. When the mixing ratio X_g is located in region I or region V, the mixture still carries more net charges, positive or negative. Mixing oppositely charged surfactants weakens the electrostatic repulsion between surfactant molecules and causes the surfactant molecules to pack more tightly, but the extent is not enough to lead to the micelle growth and micelle transition in these two regions. The electrostatic repulsion between the headgroups makes the average packing parameter lower than 1/3. The main aggregates in these two regions are thus spherical micelles and the solutions are transparent with waterlike viscosity. When X_g is located in region II and region IV, the $C_{12}C_3C_{12}(SO_3)_2$/CTAB mixtures carry less net charges than regions I and V. Electrostatic repulsion between surfactant headgroups is greatly weakened and the packing parameter is enlarged. Therefore, the micelles grow significantly and transfer into wormlike micelles. The surfactant solutions are still transparent, but the solutions at high concentration become viscous and show shear thinning property. When X_g is located in region III, the charge ratio of the $C_{12}C_3C_{12}(SO_3)_2$/CTAB mixtures is around 1:1. The net charges are so low that the headgroups can be packed very close and the average packing parameter may become close to 1. Accordingly, wormlike micelles transfer into vesicles in this region and the solutions are clouded with very low viscosity. Although hydrophobic interaction between hydrocarbon chains as well as hydration and deionization of headgroups are all changing during the aggregate transitions, the origin is from the variation of the electrostatic interaction of the headgroups in the surfactant mixtures.

Obviously, the self-assembly ability of the $C_{12}C_3C_{12}(SO_3)_2$/CTAB mixture has been greatly improved compared with $C_{12}C_3C_{12}(SO_3)_2$ or CTAB itself. Normally, the formation of wormlike micelles requires higher surfactant concentration. It was reported that the spherical micelles of CTAB grow into rodlike micelles above ∼250 mM without addition of other initiators.[55] $C_{12}C_3C_{12}(SO_3)_2$ itself can only self-assemble into spherical micelles at the concentrations studied here. In the $C_{12}C_3C_{12}(SO_3)_2$/CTAB mixtures, long wormlike micelles were formed even at C_T = 2.0 mM, i.e., 0.08% to 0.10% in mass. So the micelle growth must take place below this concentration. In particular, the $C_{12}C_3C_{12}(SO_3)_2$/CTAB wormlike micelles also exhibit excellent viscoelastic properties as described above. To enhance the viscosity of surfactant solutions, hydrogen bond, conjugation, and complexation were always introduced to form viscoelastic wormlike micelles. However, the $C_{12}C_3C_{12}(SO_3)_2$/CTAB solution possesses high viscosity mainly through the adjustment of electrostatic interaction. In short, either $C_{12}C_3C_{12}(SO_3)_2$ or CTAB is the surfactant with very strong self-assembly ability in surfactant family. On the basis of this, their mixture moves forward to a great extent.

In addition, the $C_{12}C_3C_{12}(SO_3)_2$/CTAB mixtures do not precipitate even at 1:1 charge ratio and relative high

dx.doi.org/10.1021/jp310065y | J. Phys. Chem. B 2013, 117, 433−440

concentration. It has been found that the single-chain surfactant mixtures of sodium dodecanesulfonate (SDAS)/CTAB are prone to take place.[56,57] When the charge ratio is close to 1:1, the SDAS/CTAB mixtures precipitate even when the mole concentration is as low as 0.08% at 45 °C; however, as to the $C_{12}C_3C_{12}(SO_3)_2$/CTAB mixtures, precipitation takes place only when the concentration is higher than 0.5% at 25 °C. Even if the SDAS/CTAB mixtures are rich in SDAS or rich in CTAB, phase separation often occurs. While the $C_{12}C_3C_{12}(SO_3)_2$/CTAB mixtures form homogeneous transparent micellar solutions or vesicular solutions almost at all the molar ratios. The improvement of the mixture solubility helps to the applications of surfactant mixtures. Our previous work[43] has indicated that $C_{12}C_3C_{12}(SO_3)_2$ is soluble even binding with Ca^{2+} of high concentration and the hardness tolerance of $C_{12}C_3C_{12}(SO_3)_2$ is much higher than the corresponding single-chain surfactant sodium dodecyl sulfate (SDS). The gemini structure of $C_{12}C_3C_{12}(SO_3)_2$ and the resultant aggregate structure in aqueous solution may be responsible for the high hardness tolerance. Herein the reason is similar. On the basis of the molecular characteristic of $C_{12}C_3C_{12}(SO_3)_2$ and its strong self-assembly ability, the $C_{12}C_3C_{12}(SO_3)_2$/CTAB mixtures form vesicles in aqueous solution instead of precipitation around 1:1 charge ratio.

CONCLUSION

In this work, reversible aggregate transitions from spherical micelles to wormlike micelles, vesicles, and then back to wormlike micelles and spherical micelles have been realized in the mixed anionic/cationic surfactant system of an anionic gemini surfactant $C_{12}C_3C_{12}(SO_3)_2$ and a cationic single-chain surfactant CTAB. Turbidity, rheology, DLS, Cryo-TEM, and ITC were applied to study these transitions. The results support each other and clearly present the transition process and interaction mechanism. With the variation of the mixing ratio, the five aggregate regions display clearly distinguished phase boundaries so that the aggregate regions can be well controlled. Moreover, the self-assembly ability of the $C_{12}C_3C_{12}(SO_3)_2$/CTAB mixtures is greatly improved compared with both the individual surfactants. Through adjustment of anionic/cationic charge ratio, i.e., electrostatic interaction, long wormlike micelles form at quite low concentration. In particular, the wormlike micelles show high viscoelastic property. In addition, the $C_{12}C_3C_{12}(SO_3)_2$/CTAB mixtures do not precipitate even at 1:1 charge ratio and relative high concentration. One of the greatest disadvantages of anionic/cationic surfactant mixtures is that the mixtures are very easy to precipitate, which greatly limits their applications. The present study provides an excellent system with high solubility and strong self-assembly ability. It also suggests that applying gemini surfactant should be an effective approach to improve the solubility of anionic/cationic surfactant mixtures and in turn may promote applications of the surfactant mixtures.

AUTHOR INFORMATION

Corresponding Author

*E-mail: yilinwang@iccas.ac.cn.

Notes

The authors declare no competing financial interest.

ACKNOWLEDGMENTS

This work was supported by the Chinese Academy of Sciences and National Natural Science Foundation of China (Grants 21025313, 21021003, 20973181, KJCX1-YW-21-02). We appreciate the State Key Laboratory of Polymer Physics and Chemistry for providing the DLS equipment and Key Laboratory of Polymer Chemistry and Physics of Ministry of Education in the Peking University for reological measurement.

REFERENCES

(1) Kaler, E. W.; Zana, R. *Giant Micelles: Properties and Applications*; CRC Press/Taylor & Francis: New York, 2007.
(2) Jiang, Y. *Curr. Opin. Colloid Interface Sci.* **2002**, *7*, 276−281.
(3) Walker, L. M. *Curr. Opin. Colloid Interface Sci.* **2001**, *6*, 451−456.
(4) Magid, L. J. *J. Phys. Chem. B* **1998**, *102*, 4064−4074.
(5) Koehler, R. D.; Raghavan, S. R.; Kaler, E. W. *J. Phys. Chem. B* **2000**, *104*, 11035−11044.
(6) Acharya, D. P.; Kunieda, H. *Curr. Opin. Colloid Interface Sci.* **2006**, *123*, 401−413.
(7) Hu, Y. T.; Boltenhagen, P.; Pine, D. J. *J. Rheol.* **1998**, *42*, 1185−1208.
(8) Zana, R. *Adv. Colloid Interface Sci.* **2002**, *97*, 205−253.
(9) Croce, V.; Cosgrove, T.; Dreiss, C. A. *Langmuir* **2004**, *20*, 7984−7990.
(10) Clausen, T. M.; Vinson, P. K.; Minter, J. R.; Davis, H. T.; Talmon, Y.; Miller, W. G. *J. Phys. Chem.* **1992**, *96*, 474−484.
(11) Flood, C.; Dreiss, C. A.; Croce, V.; Cosgrove, T. *Langmuir* **2005**, *21*, 7646−7652.
(12) Ziserman, L.; Abezgauz, L.; Ramon, O.; Raghavan, S. R.; Danino, D. *Langmuir* **2009**, *25*, 10483−10489.
(13) Qiao, Y.; Lin, Y. Y.; Wang, Y. j.; Li, Z. B.; Huang, J. B. *Langmuir* **2011**, *27*, 1718−1723.
(14) Cohen, D. E.; Thurston, G. M.; Chamberlin, R. A.; Benedek, G. B.; Carey, M. C. *Biochemistry* **1998**, *37*, 14798−14814.
(15) Zhu, Z.; Gonzalez, Y. I.; Xu, H.; Kaler, E. W.; Liu, S. *Langmuir* **2006**, *22*, 949−955.
(16) Israelachvili, J. N.; Mitchell, D. J.; Ninham, B. W. *J. Chem. Soc., Faraday Trans.* **1976**, *72*, 1525−1568.
(17) Kumar, R.; Kalur, G. C.; Ziserman, L.; Danino, D.; Raghavan, S. R. *Langmuir* **2007**, *23*, 12849−12856.
(18) Chu, Z.; Feng, Y.; Su, X.; Han, Y. *Langmuir* **2010**, *26*, 7783−7791.
(19) Davies, T. S.; Ketner, A. M.; Raghavan, S. R. *J. Am. Chem. Soc.* **2006**, *128*, 6669−6675.
(20) Nakamura, K.; Shikata, T. *Langmuir* **2006**, *22*, 9853−9859.
(21) Takeda, M.; Kusano, T.; Matsunaga, T.; Endo, H.; Shibayama, M. *Langmuir* **2011**, *27*, 1731−1738.
(22) Rehage, H.; Hoffmann, H. *J. Phys. Chem.* **1988**, *92*, 4712−4719.
(23) Kern, F.; Lemarechal, P.; Candau, S. J.; Cates, M. E. *Langmuir* **1992**, *8*, 437−440.
(24) Lin, Y.; Han, X.; Huang, J.; Fu, H.; Yu, C. *J. Colloid Interface Sci.* **2009**, *330*, 449−455.
(25) Raghavan, S. R.; Fritz, G.; Kaler, E. W. *Langmuir* **2002**, *18*, 3797−3803.
(26) Koshy, P.; Aswal, V. K.; Venkatesh, M.; Hassan, P. A. *J. Phys. Chem. B* **2011**, *115*, 10817−10825.
(27) Lin, Y.; Han, X.; Cheng, X. H.; Huang, J. B.; Liang, D.; Yu, C. *Langmuir* **2008**, *24*, 13918−13924.
(28) Holland, P. M.; Rubingh, D. N. *J. Phys. Chem.* **1983**, *87*, 1984−1990.
(29) Hao, L. S.; Deng, Y. T.; Zhou, L. S.; Ye, H.; Nan, Y. Q.; Hu, P. *J. Phys. Chem. B* **2012**, *116*, 5213−5225.
(30) Sohrabi, B.; Gharibi, H.; Tajik, B.; Javadian, S.; Hashemianzadeh, M. *J. Phys. Chem. B* **2008**, *112*, 14869−14876.
(31) Hoffmann, H.; Poessnecker, G. *Langmuir* **1994**, *10*, 381−389.
(32) Din, K.; Sheikh, M. S.; Dar, A. A. *J. Phys. Chem. B* **2010**, *114*, 6023−6032.

(33) Holland, P. M.; Rubingh, D. N. *Mixed Surfactant Systems*; ACS Symposium Series; American Chemical Society: Washington, DC, 1992.
(34) Bhattacharya, S.; De, S.; Subramanian, M. *J. Org. Chem.* **1998**, *63*, 7640−7651.
(35) Bhattacharya, S.; De, S. *Chem. Commun.* **1996**, 1283−1284.
(36) Bhattacharya, S.; De, S. *J. Chem. Soc., Chem. Commun.* **1995**, 651−652.
(37) Bhattacharya, S.; De, S. *Langmuir* **1999**, *15*, 3400−3410.
(38) Aswal, V. K.; Haldar, J.; De, S.; Goyald, P. S.; Bhattacharya, S. *Phys. Chem. Chem. Phys.* **2003**, *5*, 907−910.
(39) Menger, F. M.; Keiper, J. S. *Angew. Chem., Int. Ed.* **2000**, *39*, 1906−1920.
(40) Zana, R. *Curr. Opin. Colloid Interface Sci.* **1996**, *1*, 566−571.
(41) Zana, R.; Talmon, Y. *Nature* **1993**, *362*, 228−230.
(42) Wang, Y. X.; Han, Y. C.; Huang, X.; Cao, M. W.; Wang, Y. L. *J. Colloid Interface Sci.* **2008**, *319*, 534−541.
(43) Yu, D. F.; Wang, Y. X.; Zhang, J.; Tian, M. Z.; Han, Y. C.; Wang, Y. L. *J. Colloid Interface Sci.* **2012**, *381*, 83−88.
(44) Tornblom, M.; Henriksson, U.; Ginley, M. *J. Phys. Chem.* **1994**, *98*, 7041−7051.
(45) Han, Y. C.; Wang, Y. L. *Phys. Chem. Chem. Phys.* **2011**, *13*, 1939−1956.
(46) Papenmeier, G, J.; Campagnoli, J. M. *J. Am. Chem. Soc.* **1969**, *91*, 6579−6584.
(47) Taylor, J. F.; Thomas, R. K.; Penfold, J. *Adv. Colloid Interface Sci.* **2007**, *132*, 69−110.
(48) Hansson, P.; Lindman, B. *Curr. Opin. Colloid Interface Sci.* **1996**, *1*, 604−613.
(49) Tama, K. C.; Jones, E. *Chem. Soc. Rev.* **2006**, *35*, 693−709.
(50) Norvaisas, P.; Petrauskas, V.; Matulis, D. *J. Phys. Chem. B* **2012**, *116*, 2138−2144.
(51) Tarafdar, P. K.; Reddy, S. T.; Swamy, M. J. *J. Phys. Chem. B* **2010**, *114*, 13710−13717.
(52) Majhi, P. R.; Blume, A. *J. Phys. Chem. B* **2002**, *106*, 10753−10763.
(53) Bhattacharya, S.; Haldar, J. *Langmuir* **2004**, *20*, 7940−7947.
(54) Bhattacharya, S.; Haldar, J. *Langmuir* **2005**, *21*, 5747−5751.
(55) Harada, S.; Fujita, N.; Sano, T. *J. Am. Chem. Soc.* **1988**, *110*, 8710−8711.
(56) Hao, L.; Gui, Y.; Chen, Y.; He, S.; Nan, Y.; You, Y. *J. Phys. Chem. B* **2012**, *116*, 10330−10341.
(57) You, Y.; Hao, L.; Nan, Y. *Colloids Surf., A* **2009**, *335*, 154−167.